

# SLUM-i: Semi-supervised Learning for Urban Mapping of Informal Settlements and Data Quality Benchmarking

Muhammad Taha Mukhtar<sup>1,2</sup>, Syed Musa Ali Kazmi<sup>1</sup>, Khola Naseem<sup>1</sup>, Muhammad Ali Chattha<sup>1,2</sup>, Andreas Dengel<sup>1</sup>, Sheraz Ahmed<sup>1</sup>, Muhammad Naseer Bajwa<sup>1</sup>, Muhammad Imran Malik<sup>1,2,\*</sup>

<sup>1</sup>*National University of Sciences and Technology (NUST), Islamabad, Pakistan*

<sup>2</sup>*German Research Center for Artificial Intelligence (DFKI), Kaiserslautern, Germany*

## Abstract

Rapid urban expansion has fueled the growth of informal settlements in major cities of low- and middle-income countries, with Lahore and Karachi in Pakistan and Mumbai in India serving as prominent examples. However, large-scale mapping of these settlements is severely constrained not only by the scarcity of annotations but by inherent data quality challenges, specifically high spectral ambiguity between formal and informal structures and significant annotation noise. We address this by introducing a benchmark dataset for Lahore, constructed from scratch, along with companion datasets for Karachi and Mumbai, which were derived from verified administrative boundaries, totaling 1,869 km<sup>2</sup> of area. To evaluate the global robustness of our framework, we extend our experiments to five additional established benchmarks, encompassing eight cities across three continents, and provide comprehensive data quality assessments of all datasets. We also propose a new semi-supervised segmentation framework designed to mitigate the class imbalance and feature degradation inherent in standard semi-supervised learning pipelines. Our method integrates a Class-Aware Adaptive Thresholding mechanism that dynamically adjusts confidence thresholds to prevent minority class suppression and a Prototype Bank System that enforces semantic consistency by anchoring predictions to historically learned high-fidelity feature representations. Extensive experiments across a total of eight cities spanning three continents demonstrate that our approach outperforms state-of-the-art semi-supervised baselines. Most notably, our method demonstrates superior domain transfer capability whereby a model trained on only 10% of source labels reaches a 0.461 mIoU on unseen geographies and outperforms the zero-shot generalization of fully supervised models.

**Keywords:** Semi-Supervised Learning, Semantic Segmentation, Remote Sensing, Informal Settlements, Slum Detection

## 1. Introduction

Rapid urbanization in low- and middle-income countries is driving unprecedented demographic shifts, with urban areas now housing 55% of the global population, a figure projected to reach 68% by 2050 [1]. This rapid growth outpaces the capacity of formal housing markets and urban infrastructure, forcing many to settle in informal neighborhoods lacking adequate legal protection and basic services. Informal settlements, as defined by the United Nations [2], are urban areas exhibiting one or more of the following: (i) insecure legal tenure for land or housing, (ii) insufficient access to formal infrastructure and basic services, and (iii) non-compliance with planning or building regulations. Such settlements are often located in environmentally vulnerable areas.

In Pakistan, urban slums house millions, yet remain largely unaccounted for in official datasets. A 2020 UNICEF study [3] across 10 major cities found that only 53% of children in slums receive full immunization, over 56% live in vulnerable housing, and 70% of mothers have five or fewer years of education. These conditions underscore the need for targeted interventions

and robust mapping, as the informal nature of such settlements hinders effective policy and service delivery.

Traditional surveys often fail to capture the full extent of informal settlements. Remote sensing provides a scalable alternative by using semantic segmentation to label each pixel in satellite imagery, enabling precise and comprehensive mapping. Existing methods include spectral indices such as NDBI [4] and UI [5], machine learning approaches like SVMs and Random Forests [6, 7, 8], and deep learning approaches for large-scale mapping [9, 10]. While semantic segmentation effectively captures complex settlement structures, it requires large, high-quality annotated datasets that Pakistani cities lack.

Our contributions are threefold. First, we release the first verified high-resolution semantic segmentation dataset for Lahore, Pakistan, validated against official directorate records alongside standardized benchmarks for Karachi and Mumbai. Second, we propose a novel framework that addresses the inherent limitations of generic semi-supervised learning (SSL) methods in high-imbalance geospatial tasks through Class-Aware Adaptive Thresholding and a Prototype Bank. Third, we provide a rigorous evaluation of foundation models in semi-supervised learning, demonstrating that foundation models enhanced by SSL (specifically our method adapted for DINOv2 [11]) achieve superior zero-shot transfer performance across unseen cities com-

\*Corresponding author.

pared to general fully supervised foundation model baselines.

## 2. Data Acquisition and Processing

Given the susceptibility of major urban centers to overcrowding and informal settlement expansion, this study focuses on three of the most populous cities in South Asia: Karachi and Lahore in Pakistan, and Mumbai in India. Data acquisition prioritized high-quality annotations for slums. For Lahore, we collaborated with the Katchi Abadis (Informal Settlements) Directorate to secure the official registry of informal settlements. Two annotators manually delineated 266 polygons, validating boundaries against Google Earth Pro [12] imagery and visual cues. Discrepancies were resolved through a joint review of contextual indicators and official records. For Karachi and Mumbai, datasets were derived from high-resolution satellite imagery and publicly available annotations [13, 14]. The final study areas encompass 171 km<sup>2</sup> (Lahore), 516 km<sup>2</sup> (Mumbai), and 1,182 km<sup>2</sup> (Karachi), with selection focused on regions where slums are most densely clustered.

Using these verified boundaries, satellite imagery was extracted from Google Earth Pro at zoom level 19, which aggregates multiple high-resolution sources ( $\approx 30\text{--}50$  cm). RGB rasters were extracted in the EPSG:4326 coordinate system via Leafmap [15] and tiled into 512  $\times$  512 image-mask pairs. To rigorously evaluate model robustness across heterogeneous geographic contexts, we also leverage five established datasets from prior studies on African (Makoko, El Geneina, El Daein, Northern Nairobi) and South American (Medellin) cities [16].

### 2.1. Dataset Complexity Analysis

To quantify the challenges inherent in these datasets, we employ three complementary metrics. First, Boundary Complex-

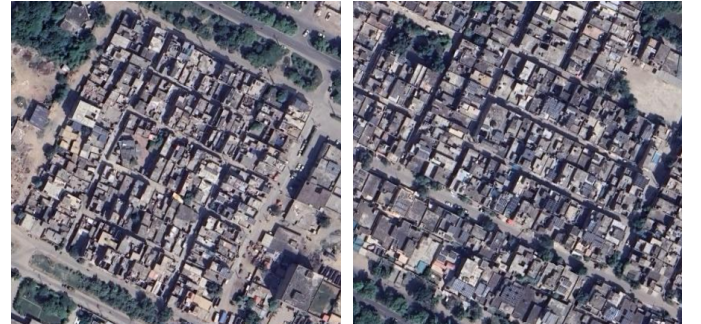


Figure 2: Visual comparison of feature contrast between Zia Colony, Lahore, a verified informal settlement [18] (left), and Township, Lahore, a formal planned development (right). Images from Google Earth Pro [12]

ity, measured via fractal dimension [17], which quantifies geometric irregularity and higher values indicate intricate perimeters that are significantly harder to delineate. Second, Feature Contrast assesses visual discriminability via Signal-to-Noise Ratio (SNR). A low SNR ( $< 2$ ) implies that slum features and the background are roughly indistinguishable, whereas a high SNR ( $> 8$ ) reflects strong contrast against non-slum regions. Finally, Label-to-Signal Divergence measures the alignment between annotated boundaries and actual image gradients; high displacement values in this metric identify areas where labels likely rely on non-visual context rather than observable edges.

We characterize the heterogeneity of our evaluation benchmark by analyzing datasets across these dimensions. As shown in Figure 1, the resulting SNR spectrum reveals substantial variation. External datasets range from highly ambiguous (El Daein, SNR = 1.0) to exceptionally high-contrast (Makoko, SNR = 20.5), while our South Asian datasets span medium-to high-contrast zones: Lahore (SNR = 5.7), Karachi (SNR = 12.9), and Mumbai (SNR = 14.8). Lahore's lower SNR reflects the subtle visual distinctions characteristic of mixed formal-informal neighborhoods common in Lahore.

As illustrated in Figure 2, the use of similar construction materials and incremental development patterns reduces feature

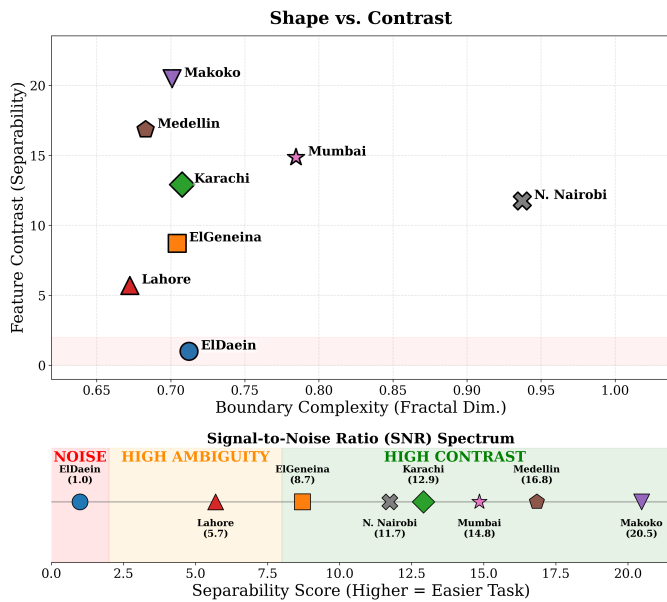


Figure 1: Dataset characterization across boundary complexity, feature contrast, and signal-to-noise ratio dimensions.

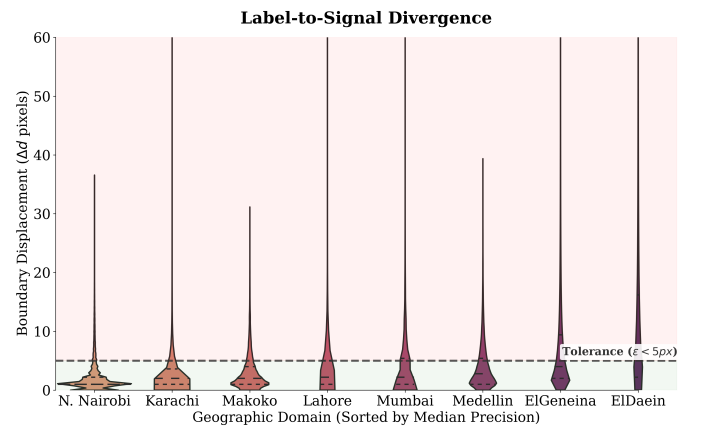


Figure 3: Annotation precision measured by boundary displacement relative to image gradients across all datasets. Narrow distributions indicate high consistency.

City	Slum	Non-Slum	Mixed	Total
El Daein	522	1,508	555	2,585
El Geneina	193	1,208	535	1,936
N. Nairobi	0	58	53	111
Medellin	3	8	24	35
Makoko	0	25	41	66
Mumbai	29	19,969	4,842	24,840
Lahore	468	8,439	1,043	9,950
Karachi	215	33,863	2,171	36,249

Table 1: Tile distribution across full datasets.

contrast in these regions. The scatter plot (Figure 1) further reveals that boundary complexity and feature contrast vary independently; some datasets exhibit simple boundaries but poor visual separation (Lahore), while others combine complex geometries with strong visual cues (Karachi).

To validate annotation precision, Figure 3 visualizes the distribution of boundary displacement relative to image gradients. A tolerance threshold of 5 pixels (dashed line) marks the limit for acceptable alignment with visual transitions. The results demonstrate that the Lahore dataset maintains a tight distribution with minimal outliers, despite its low-contrast visual characteristics. Conversely, datasets with elongated tails indicate greater ambiguity in boundary delineation.

## 2.2. Benchmarking Strategy and Subset Creation

The class distribution across both the newly generated South Asian datasets and those sourced from prior literature is presented in Table 2.1. We categorize tiles into three distinct classes, defining Slum as tiles exclusively comprising informal settlement pixels, Non-Slum as those exclusively comprising background or formal pixels, and Mixed as tiles containing both slum and non-slum regions. As observed, the tiling process yields extensive datasets for the target cities, particularly Karachi and Mumbai.

However, the sheer size of these three datasets necessitates an assessment of their practicality for semi-supervised benchmarking. Training directly on the full corpus with even modest annotation budgets (e.g., 10% of tiles labeled, and the rest assumed as unlabeled) results in performance saturation [19], which precludes the effective assessment of semi-supervised improvements. To establish an evaluation regime where label efficiency is critical, we simulate annotation scarcity by creating stratified subsets of 1,000 tiles per city (Table 2.2). Given the severe under-representation of pure slum tiles in these subsets, we employ data augmentation to prevent minority class

City	Slum	Non-Slum	Mixed	Total
Mumbai	1	804	195	1,000
Lahore	47	848	105	1,000
Karachi	6	934	60	1,000

Table 2: Stratified tile distribution across reduced datasets.

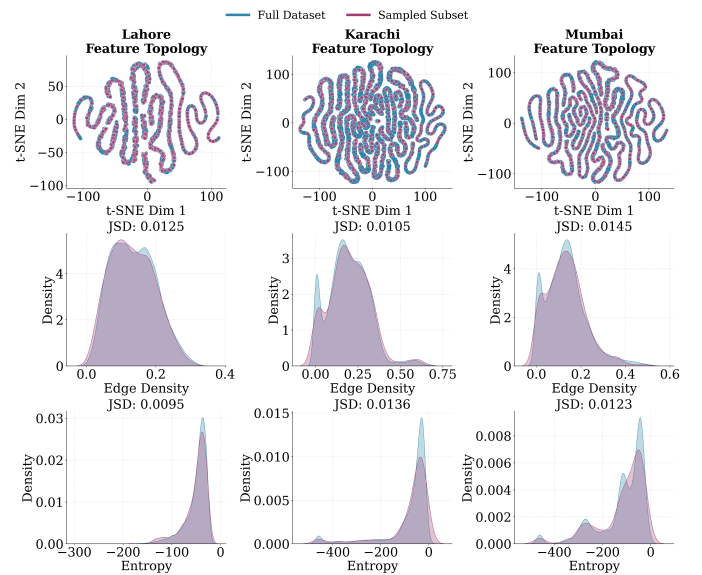


Figure 4: Representativeness analysis across three cities (Lahore, Karachi, Mumbai). The t-SNE feature topologies, edge density, and entropy distributions show that the **sampled subset** accurately preserves the characteristics of the **full dataset**.

collapse during training.

To guard against selection bias in the 1,000-tile subsets and verify that they accurately reflect the full city distributions, we assess representativeness using complementary feature- and distribution-level checks. We compute (i) t-SNE embeddings [20] of PCA-reduced entropy and edge features; (ii) edge density from thresholded Sobel gradients; and (iii) grayscale entropy. Jensen–Shannon distances (JSD) [21] quantify the divergence between full and reduced datasets. Figure 4 confirms that, across Lahore, Mumbai, and Karachi, the subsets occupy the same t-SNE manifolds as the full datasets and display nearly identical edge-density and entropy profiles. While these checks cannot establish full equivalence, they confirm that the reduced datasets preserve sufficient diversity to serve as controlled, limited-label benchmarks.

## 2.3. Dataset Partitioning

We partition the datasets into training (80%) and testing (20%) sets. 10% of the training partition is held out for validation, resulting in an effective global distribution of 72% training, 8% validation, and 20% testing.

For the SSL experiments, we define three scarcity protocols

Protocol	Labeled ( $D_L$ )	Unlabeled ( $D_U$ )
10% Label	10%	90%
20% Label	20%	80%
30% Label	30%	70%

Table 3: SSL experimental protocols. The training data ( $D_{train}$ ) is partitioned into labeled ( $D_L$ ) and unlabeled ( $D_U$ ) sets. To ensure consistency, labeled subsets are nested, meaning larger sets contain the smaller ones ( $D_L^{10\%} \subset D_L^{20\%} \dots$ ).

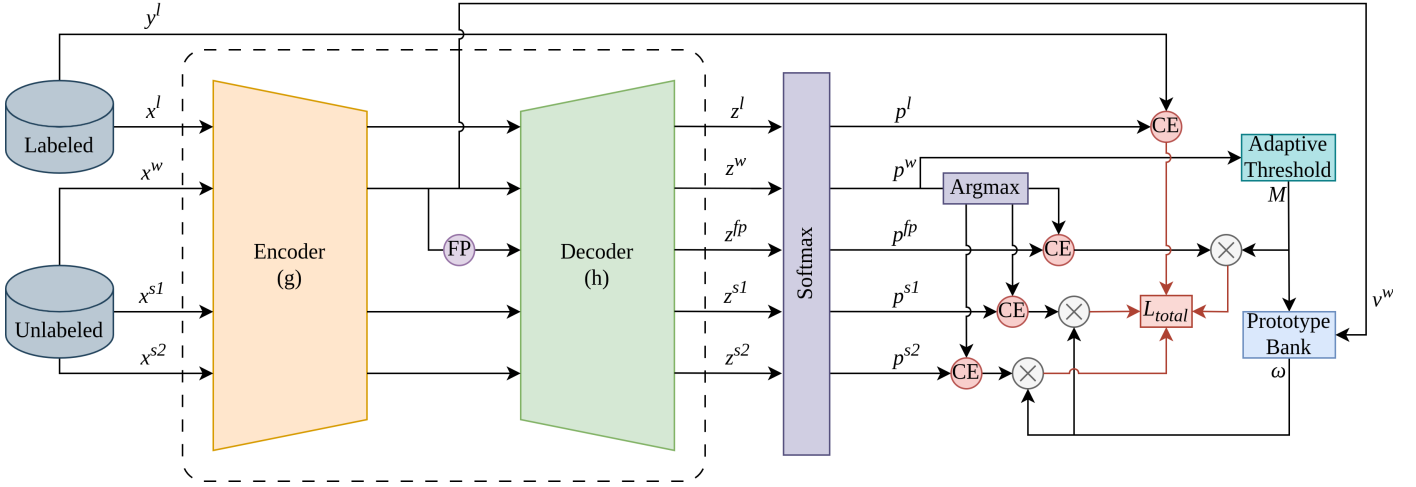


Figure 5: Overview of the proposed semi-supervised framework. The pipeline consists of a shared encoder-decoder network processing labeled ( $x^l$ ), weak ( $x^w$ ), and strong ( $x^{s1}, x^{s2}$ ) views.

by withholding ground-truth annotations within the training set, as detailed in Table 2.3. We simulate scenarios with 10%, 20%, and 30% labeled data, treating the remaining portions as unlabeled. Crucially, we employ a nested sampling strategy; for instance, the 20% labeled subset is a strict superset of the 10% subset. This ensures that performance improvements across protocols are driven by the addition of new data points rather than variations in the sample distribution.

### 3. Methodology

The proposed framework extends the UniMatch pipeline [22], SSL architecture utilizing a DeepLabV3+ [23] encoder-decoder backbone. While UniMatch demonstrates state-of-the-art performance on generic computer vision benchmarks, its efficacy diminishes in the context of informal settlement detection. We observe that the extreme class imbalance inherent to slum mapping, characterized by a critically low slum-to-background pixel ratio, prevents the model from consistently surpassing the static confidence threshold ( $\tau = 0.95$ ) defined in the original UniMatch formulation. Consequently, high-quality slum features are frequently discarded, leading to a degradation in performance that can sometimes fall below purely supervised baselines.

To address these limitations, we introduce two modular components designed to stabilize training and minimize degradation in Slum detection settings, as illustrated in Figure 5:

1. A dynamic gating mechanism that replaces the static confidence requirement with a class-specific confidence threshold.
2. A memory-efficient queue storing high-fidelity feature representations. This generates a reliability weight  $\omega$  by verifying whether a current prediction aligns with historically learned representations of informal settlements.

#### 3.1. Baseline Framework

Our method is inspired by UniMatch, which adapts the FixMatch [24] weak-to-strong consistency framework. The training process operates on a single network architecture consisting of an encoder  $g(\cdot)$  and a decoder  $h(\cdot)$ , processing labeled and unlabeled data streams. For an input  $x$ , we denote the intermediate feature embedding as  $v = g(x)$  and the final output logits as  $z = h(v)$ . The softmax probability is  $p = \text{softmax}(z)$ .

For the supervised component, a labeled image  $x^l$  is passed through the model to generate logits  $z^l$ , which are processed via softmax to produce  $p^l$ . The supervised loss  $\mathcal{L}_{\text{sup}}$  is then calculated as the standard cross-entropy between  $p^l$  and the ground-truth label  $y^l$ .

The unsupervised component enforces consistency across different perturbations of the same input. An unlabeled image  $x^u$  first undergoes weak augmentation to obtain  $x^w$ . The model predicts logits  $z^w = h(g(x^w))$ , where the softmax probability  $p^w = \text{softmax}(z^w)$  serves as the source for pseudo-label generation. To enforce consistency, the same image simultaneously undergoes strong augmentation (specifically CutMix [25]) to generate two views,  $x^{s1}$  and  $x^{s2}$ . The model is then optimized to align the predictions from these strongly distorted inputs with the pseudo-labels derived from the weak view  $x^w$ . Additionally, a Feature Perturbation (FP) mechanism injects noise into the encoder features of the weak view to produce  $z^{fp}$ , further enforcing internal feature robustness.

#### 3.2. Class-Aware Adaptive Thresholding (CAAT)

Standard UniMatch [22] relies on a fixed global threshold ( $\tau = 0.95$ ). This approach disproportionately suppresses the minority class where, as demonstrated in Table 2.1 and Table 2.2, the class imbalance is significant. To mitigate this, we introduce CAAT, a dynamic mechanism inspired by FreeMatch [26]. We maintain a class-specific threshold vector  $\mathcal{T} \in \mathbb{R}^C$ , where  $C$  is the total number of classes. At each iteration  $t$ , we compute the mean confidence  $\mu_c^{(t)}$  for each class

$c \in \{1, \dots, C\}$  present in the current batch. The threshold is updated via Exponential Moving Average (EMA):

$$\mathcal{T}_c^{(t)} = \beta \cdot \mathcal{T}_c^{(t-1)} + (1 - \beta) \cdot \mu_c^{(t)} \quad (1)$$

where  $\beta = 0.999$  is the momentum coefficient. To prevent trivial solutions or excessive filtering, we enforce a valid range using a clipping function:

$$\tau_c^{(t)} = \text{Clip}(\mathcal{T}_c^{(t)}, \tau_{min}, \tau_{max}) \quad (2)$$

We define the range  $[\tau_{min}, \tau_{max}] = [0.6, 0.95]$ . We adopt the upper bound  $\tau_{max} = 0.95$  following standard protocols in semi-supervised learning [24, 22, 27]. The lower bound is set to  $\tau_{min} = 0.6$  to ensure that pseudo-labels remain informative while allowing the model to learn from harder examples that are rejected by the static threshold.

Finally, we generate a binary mask  $M \in \{0, 1\}^{H \times W}$  that determines which pixels contribute to the unsupervised loss. For a pixel at position  $(i, j)$  with predicted class  $\hat{y}_{i,j}$  and confidence  $p_{i,j}^w$ , the mask is defined as:

$$M_{i,j} = \mathbb{1}(\max(p_{i,j}^w) \geq \tau_{\hat{y}_{i,j}}^{(t)}) \quad (3)$$

where  $\mathbb{1}(\cdot)$  is the indicator function.

This establishes a dynamic curriculum, admitting lower-confidence slum predictions early in training while demanding higher fidelity as the model approaches convergence.

### 3.3. Prototype Bank System

While CAAT addresses the quantity of pseudo-labels by dynamically adjusting confidence thresholds, it does not guarantee their semantic quality. High-confidence false positives remain common in ambiguous regions, such as dense formal housing resembling slums. To penalize these semantically divergent predictions, we introduce a Prototype Bank that explicitly models the global feature distribution of both background and informal settlement classes.

We maintain a feature queue  $\mathcal{Q} = \{\mathcal{Q}_c\}_{c=1}^C$ , where each  $\mathcal{Q}_c$  stores  $K = 2000$  normalized feature vectors of dimension  $d = 256$  (matching the standard output of the DeepLabV3+ projection head). The bank is dynamically updated using features  $v^w = g(x^w)$  from the weakly augmented view. To ensure the purity of the stored prototypes, we strictly populate  $\mathcal{Q}$  using only those pixels that successfully pass the CAAT mask ( $M_{i,j} = 1$ ). Formally, for a specific class  $c$ , we collect the set of valid feature vectors:

$$\mathcal{V}_c = \{v_{i,j}^w \mid \hat{y}_{i,j} = c \wedge M_{i,j} = 1\} \quad (4)$$

These vectors are randomly subsampled to maintain batch diversity, normalized, and pushed into the respective class queue via a First-In-First-Out (FIFO) mechanism.

Leveraging this global context, we derive a reliability weight  $\omega$  to modulate the unsupervised loss. For every pixel in the training batch, we verify if its current feature representation  $v_{i,j}^w$  aligns with the historical prototypes of its predicted class. This

is computed via the maximum cosine similarity between the current feature and the stored prototypes in  $\mathcal{Q}_{\hat{y}_{i,j}}$ :

$$\omega_{i,j} = \left( \max_{k \in [1, K]} \langle v_{i,j}^w, \mathcal{Q}_{\hat{y}_{i,j}, k} \rangle \right)^\gamma \quad (5)$$

where  $\gamma = 2.0$  is a scaling factor that suppresses contributions from features distant from the cluster center. As illustrated in Figure 5, this weight  $\omega$  is applied to the strong augmentation stream to penalize inconsistent features, and it is not applied to the Feature Perturbation (FP) stream, as the FP objective targets internal decoder robustness against noise rather than strict semantic consistency with the global distribution.

### 3.4. Total Objective Function

The total unsupervised loss is a weighted sum of the Strong Augmentation loss ( $\mathcal{L}_s$ ) and the Feature Perturbation loss ( $\mathcal{L}_{fp}$ ). For the strong views ( $s \in \{s1, s2\}$ ), the loss is gated by the binary mask  $M$  and weighted by the reliability  $\omega$  and  $|\mathcal{P}|$  is the total number of pixels:

$$\mathcal{L}_s = \frac{1}{|\mathcal{P}|} \sum_{(i,j) \in \mathcal{P}} \underbrace{\omega_{i,j} \cdot M_{i,j}}_{\text{Gating}} \cdot \ell_{ce}(p_{i,j}^s, \hat{y}_{i,j}) \quad (6)$$

For the feature perturbation stream, only the adaptive threshold mask  $M$  is applied:

$$\mathcal{L}_{fp} = \frac{1}{|\mathcal{P}|} \sum_{(i,j) \in \mathcal{P}} M_{i,j} \cdot \ell_{ce}(p_{i,j}^{fp}, \hat{y}_{i,j}) \quad (7)$$

The final training objective combines the supervised and unsupervised components:

$$\mathcal{L}_{total} = \frac{1}{2}(\mathcal{L}_{sup} + \frac{1}{2}(\mathcal{L}_{s1} + \mathcal{L}_{s2}) + \frac{1}{4}\mathcal{L}_{fp}) \quad (8)$$

This formulation ensures that the model learns from samples that are both confident (via CAAT) and semantically consistent (via Prototype Bank), while maintaining feature robustness through perturbation.

## 4. Experiments

### 4.1. Experimentation Details

The proposed framework was implemented in PyTorch and trained on NVIDIA RTX A6000 GPUs. We maintain a consistent data augmentation pipeline, including random horizontal flipping and scaling (0.8 to 1.2 $\times$ ).

Our primary experiments utilize a ResNet-101 [28] backbone with a DeepLabV3+ [23] head. We train for 80 epochs with a batch size of 8 and a crop size of 512 $\times$ 512. We employ the SGD optimizer with a momentum of 0.9, a weight decay of  $1 \times 10^{-4}$ , and an initial learning rate ( $\eta$ ) of 0.02.

To evaluate the modularity of our approach within the current paradigm of foundation models and self-supervised representation learning, we integrated our framework into the UniMatch-v2 [27] pipeline. This configuration employs a DINoV2-small [11] backbone coupled with a DPT [29] decoder. Following the standard UniMatch-v2 protocol, we utilized a crop

Budget Method	EXTERNAL BENCHMARKS					PROPOSED BENCHMARKS			
	El Daein	El Geneina	N. Nairobi	Makoko	Medellin	Mumbai	Lahore	Karachi	
10%	Supervised	0.524	<u>0.667</u>	0.647	0.158	0.150	0.726	<b>0.785</b>	<b>0.629</b>
	FixMatch [24]	0.674	0.641	0.649	<b>0.619</b>	0.715	<b>0.755</b>	<u>0.730</u>	<u>0.589</u>
	UniMatch [22]	<b>0.702</b>	0.625	<b>0.710</b>	0.560	<u>0.871</u>	<u>0.728</u>	0.711	0.508
	<b>Ours</b>	0.680	<b>0.720</b>	0.709	0.589	<b>0.908</b>	0.719	0.695	0.584
	Supervised <sup>†</sup>	<u>0.691</u>	0.652	0.690	0.208	0.227	0.739	0.719	<b>0.631</b>
	UniMatch-v2 [27] <sup>†</sup>	<b>0.692</b>	<u>0.686</u>	<u>0.713</u>	<b>0.419</b>	<u>0.868</u>	<u>0.780</u>	<b>0.750</b>	0.615
20%	<b>Ours</b> <sup>†</sup>	0.680	<b>0.691</b>	<u>0.717</u>	0.413	<b>0.899</b>	<b>0.783</b>	0.728	<u>0.626</u>
	Supervised	0.707	0.700	<u>0.723</u>	0.158	0.150	0.713	<u>0.758</u>	0.485
	FixMatch [24]	<u>0.715</u>	0.708	0.710	0.580	<u>0.859</u>	0.720	<b>0.768</b>	<u>0.540</u>
	UniMatch [22]	<b>0.728</b>	<u>0.726</u>	<b>0.733</b>	0.618	0.814	<b>0.764</b>	0.757	<b>0.565</b>
	<b>Ours</b>	0.702	<b>0.747</b>	0.722	<b>0.659</b>	<b>0.909</b>	0.748	0.754	0.483
	Supervised <sup>†</sup>	0.729	<u>0.719</u>	0.709	0.208	0.227	0.705	<b>0.750</b>	<b>0.674</b>
30%	UniMatch-v2 [27] <sup>†</sup>	<u>0.738</u>	<b>0.722</b>	<b>0.717</b>	<b>0.660</b>	<u>0.861</u>	<b>0.771</b>	0.736	0.562
	<b>Ours</b> <sup>†</sup>	<b>0.744</b>	0.713	<u>0.710</u>	<u>0.658</u>	<b>0.861</b>	0.763	<u>0.740</u>	<u>0.574</u>
	Supervised	0.677	0.699	0.725	0.158	<u>0.901</u>	0.752	0.722	<b>0.745</b>
	FixMatch [24]	<u>0.735</u>	<u>0.725</u>	0.708	<b>0.679</b>	0.802	<u>0.757</u>	<b>0.757</b>	0.683
	UniMatch [22]	0.708	<b>0.741</b>	<b>0.741</b>	0.404	0.900	0.741	0.711	<u>0.744</u>
	<b>Ours</b>	<b>0.749</b>	0.704	0.732	0.584	<b>0.925</b>	<b>0.765</b>	0.742	0.635
	Supervised <sup>†</sup>	0.727	0.703	0.698	0.208	0.878	<b>0.758</b>	0.759	0.669
	UniMatch-v2 [27] <sup>†</sup>	<u>0.744</u>	<b>0.716</b>	<b>0.729</b>	0.634	<b>0.904</b>	<u>0.758</u>	<b>0.773</b>	<b>0.739</b>
	<b>Ours</b> <sup>†</sup>	<b>0.749</b>	0.714	<u>0.719</u>	<b>0.665</b>	<u>0.892</u>	0.739	<u>0.759</u>	0.737
	<b>Fully Supervised</b>	0.752	0.723	0.747	0.740	0.881	0.766	0.809	0.553
	<b>Fully Supervised</b> <sup>†</sup>	0.801	0.748	0.708	0.485	0.947	0.780	0.825	0.775

<sup>†</sup>: Methods using DINOV2 [11] backbone.

Table 4: Mean IoU (mIoU) Results. **Bold** indicates best, underline indicates second best. Fully Supervised means experiments with 100% labeled data and no unlabeled data.

size of  $518 \times 518$  to satisfy the  $14 \times 14$  patch size alignment required by the Vision Transformer (ViT) [30] architecture. The backbone was frozen to maintain the integrity of the pre-trained features, focusing the learning on the segmentation head. Training was conducted for 60 epochs using the AdamW optimizer ( $\beta_1 = 0.9, \beta_2 = 0.999$ ) with a weight decay of 0.01. We utilize a base learning rate of  $5 \times 10^{-6}$  with a multiplier of  $40\times$ . Additionally, an EMA teacher with a decay rate of 0.996 was utilized to stabilize pseudo-labeling. Both implementations adhered strictly to the default configurations provided in the official UniMatch and UniMatch-v2 codebases. This ensures that the performance observed reflects the intrinsic extensibility of our method rather than the results of custom tuning.

#### 4.2. Quantitative Evaluation

To rigorously evaluate the proposed framework, we benchmark against state-of-the-art SSL methods, including FixMatch, UniMatch, and UniMatch-v2, alongside a supervised baseline trained strictly on the labeled subset. Experiments were conducted across eight geographically diverse cities to capture varying slum morphologies.

We evaluate performance using the Mean Intersection over Union (mIoU); results are summarized in Table 4. Our method demonstrates consistent improvements over the supervised baseline and remains competitive against established SSL frameworks. Specifically, at the 10% labeled data split, our ResNet-based configuration outperforms UniMatch in 4 out of

8 cities, while our DINOV2 adaptation surpasses UniMatch-v2 in 5 out of 8 cities. This competitive trend extends to other data regimes. At 20% labeled data, we outperform baselines in 3 (ResNet) and 4 (DINOV2) cities, and at 30% labeled data, the ResNet configuration maintains superiority in 5 cities, while DINOV2 leads in 1. Aggregating these results, our method proves to be highly competitive against the strong UniMatch baselines across diverse evaluation scenarios.

We observe a divergence in performance metrics across specific urban environments. In the ResNet configuration, our method quantitatively yields lower mIoU than UniMatch in some scenarios in Lahore, Karachi, and Mumbai. However, as detailed in Section 4.3, this numerical gap diverges from the qualitative assessment. UniMatch struggles with semantic confusion, often classifying formal settlements as slums in complex transition zones, whereas our method maintains semantic specificity. This suggests that standard mIoU metrics may not fully capture improvements in boundary adherence and semantic consistency where ground truth boundaries are inherently ambiguous. Notably, utilizing the stronger DINOV2 backbone mitigates this discrepancy to a significant extent.

Finally, in certain scenarios, we observe that semi-supervised methods underperform the supervised baseline. This is attributed to two factors detailed in Section 2.1. First, the morphological ambiguity of slums makes drawing precise boundaries difficult, introducing noise into the pseudo-labeling pro-

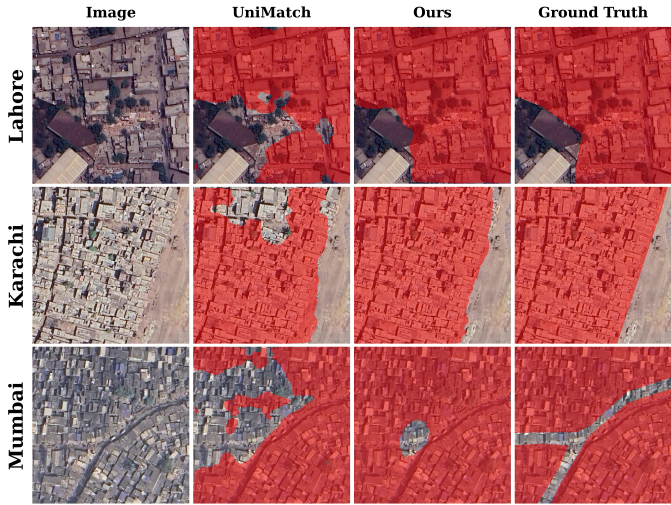


Figure 6: Qualitative comparison between the baseline (UniMatch) and our proposed method on the Lahore, Karachi, and Mumbai datasets at 10% labeled splits.

cess. Second, for smaller datasets, increasing the labeled split significantly reduces the pool of available unlabeled data, thereby diminishing the leverage of semi-supervised consistency regularization. Despite these constraints, our method demonstrates superior robustness compared to the baselines in the majority of extremely low-data regimes (e.g., Makoko and Medellin).

#### 4.3. Qualitative Analysis

To assess perceptual quality, we compare our ResNet-101 implementation against the UniMatch baseline on the Lahore, Karachi, and Mumbai datasets using the 10% labeled split. We focus on this configuration as it represents the critical low-data regime where semi-supervised learning is most vital. The visual results in Figure 6 highlight the divergence between metric-based evaluation and perceptual reality. In all three cities, the baseline exhibits significant semantic confusion and fragmentation, frequently misclassifying formal, high-density, low-rise housing as “Slum” due to textural similarities. In contrast, our Prototype Bank successfully suppresses these false positives by enforcing feature consistency with stored global prototypes. This results in cleaner decision boundaries between formal and informal zones, demonstrating that our method maintains semantic integrity even in complex morphologies where the baseline yields noisy, albeit numerically high-scoring, predictions.

#### 4.4. Prototype Bank Evolution

To validate the stability of the Prototype Bank (Section 3.3), we visualize the feature queue evolution via t-SNE in Figure 7. Initially, slum and non-slum prototypes exhibit significant overlap. However, as the reliability weight  $w$  (Eq. 5) penalizes divergent features, a clear separation emerges by the final epoch. The formation of distinct, compact clusters confirms that the memory bank acts as a “semantic anchor”.

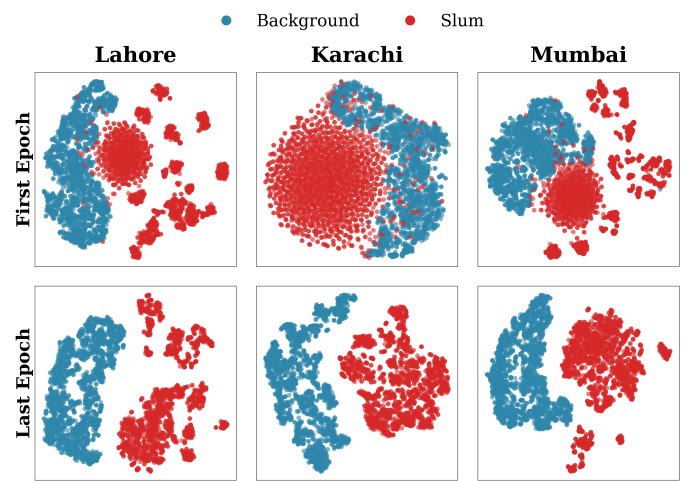


Figure 7: t-SNE visualization of vector evolution within the Prototype Bank. The plots illustrate the transition from overlapping class distributions in the first epoch to well-separated clusters by the end of training.

#### 4.5. Ablation Studies

To isolate the individual contribution of each component, we evaluated the Class-Aware Adaptive Thresholding (CAAT) and the Prototype Bank independently. We averaged performance metrics across all cities to create a unified view of algorithmic behavior. Figure 8 presents the mIoU as the labeled data split increases from 10% to 30%.

The Class-Aware Adaptive Thresholding (CAAT) module proves to be the most critical component in the data-scarce regime. At the 10% split, the CAAT-only configuration significantly outperforms the Prototype Bank-only setup. This occurs because the baseline model is often too conservative in low-data settings, filtering out valuable supervisory signals by failing to reach the static confidence threshold ( $\tau = 0.95$ ). CAAT mitigates this by dynamically adjusting requirements, allowing the model to learn from difficult examples earlier in the training

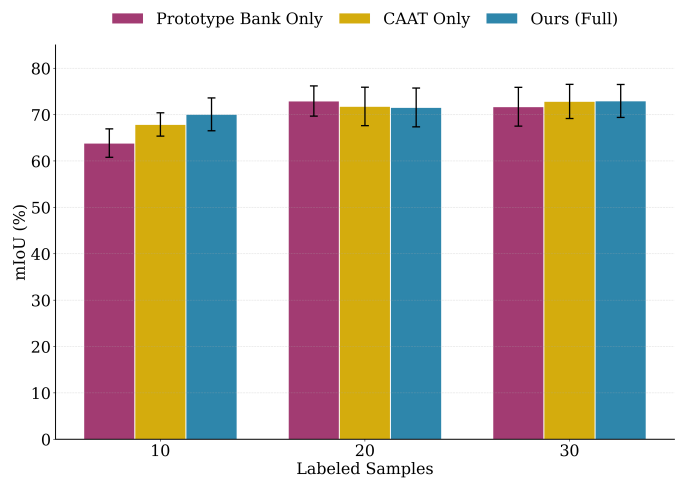


Figure 8: Component-wise ablation study showing segmentation accuracy averaged across all cities. The graph compares the Prototype Bank-only, CAAT-only, and Full Framework configurations.

trajectory.

Conversely, the Prototype Bank is less effective in isolation during the early stages of training. Due to the strict confidence threshold, the memory bank struggles to populate with features when the model is weak. Consequently, the queue retains uninformative initialization vectors for extended periods, a phenomenon particularly pronounced in the 10% setting. However, as supervision increases (20% and 30% splits), the model becomes confident enough to update the bank, and its performance contribution matches or exceeds that of CAAT.

The full framework achieves optimal stability by synergizing these strengths. Integrating both modules yields the highest performance at the 10% mark. CAAT ensures a sufficient flow of pseudo-labels to drive the learning process, while the Prototype Bank acts as a “semantic anchor,” filtering these labels to ensure consistency with the slum representations stored in the queue. The performance gap between configurations narrows at 20% and 30% as the model naturally improves with increased ground truth supervision.

#### 4.6. Computational Analysis

To ensure a fair comparison, we evaluate the computational footprint of our proposed framework against the baseline methods. Our approach maintains an identical model complexity to the baselines, with the ResNet-101 and DINOv2 configurations utilizing 59.5M and 24.2M parameters, respectively. Inference complexity remains consistent, with inference FLOPs unchanged at 96.08G (ResNet-101) and 40.45G (DINOv2).

We quantify training efficiency using the ratio of aggregate training times (total overhead) across all experimental configurations. For the ResNet-101 backbone, our approach incurs a negligible overhead of 0.65% compared to the standard UniMatch pipeline.

In the case of the DINOv2-based configuration, we observe a relative training time increase of 45.2% compared to UniMatch-v2. While this percentage appears significant, it must be viewed in the context of the high efficiency of the DINOv2 backbone. The baseline UniMatch-v2 pipeline is exceptionally fast (0.65 hours (39 minutes) average). Thus, the relative increase translates to a minor absolute time cost (averaging 0.94 hours (56 minutes) total). Crucially, our DINOv2-based method remains  $\sim 2.6\times$  faster than the standard ResNet-101 baseline (2.43 hours average).

#### 4.7. Cross-City Generalization

To assess model robustness against domain shifts, we evaluated performance on unseen cities, which represents a challenging zero-shot transfer setting given the morphological variations in informal settlements. Table 5 presents the performance metrics averaged across all cities, where our method demonstrates superior generalization capabilities compared to both supervised and semi-supervised baselines. While standard ResNet-101 configurations show consistent improvements, the efficacy of our approach is most pronounced with the DINOv2 backbone. In this setting, the baseline UniMatch-v2 suffers from class collapse, where it exclusively predicts the

Method	LABELED DATA SPLIT			REFERENCE
	10%	20%	30%	
Supervised	0.324	0.326	0.368	0.437
FixMatch [24]	<b>0.446</b>	<b>0.440</b>	0.405	–
UniMatch [22]	0.441	<u>0.435</u>	<u>0.445</u>	–
<b>Ours</b>	<b>0.447</b>	0.431	<b>0.457</b>	–
Supervised <sup>†</sup>	0.388	0.387	0.419	0.456
UniMatch-v2 [27] <sup>†</sup>	<u>0.443</u>	<u>0.443</u>	<u>0.443</u>	–
<b>Ours <sup>†</sup></b>	<b>0.461</b>	<b>0.452</b>	<b>0.461</b>	–

<sup>†</sup>: Methods using DINOv2 [11] backbone.

Table 5: Cross-City Generalization Results (Mean IoU). We report the average performance on unseen cities. **Bold** indicates best, underline indicates second best.

background class and yields identical scores across all splits, whereas our method maintains stability. Our framework yields superior performance compared to alternative semi-supervised approaches across nearly all evaluated scenarios. Furthermore, it remarkably outperforms the fully supervised baselines in both ResNet-101 and DINOv2 configurations despite utilizing significantly less data. Notably, our approach using only 10% labeled data achieves a mean IoU of 0.461 and surpasses the fully supervised DINOv2 baseline trained on 100% of the data. This confirms that our method effectively learns transferable and semantic representations rather than overfitting to source-domain textures.

## 5. Conclusion

In this work, we addressed the dual challenges of data scarcity and semantic ambiguity in the remote sensing of informal settlements. By introducing verified benchmarks for South Asian megacities and proposing a specialized semi-supervised framework, we demonstrated that effective slum mapping is achievable even with minimal annotation budgets. However, we also identified specific scenarios where the methodology fails to converge regardless of label volume, highlighting the intrinsic difficulty of the domain.

Our integration of Class-Aware Adaptive Thresholding and a Prototype Bank system successfully mitigated the static threshold limitations of prior SSL methods like UniMatch. These components prevented the suppression of minority slum classes and filtered out semantically inconsistent false positives in complex transition zones.

Despite these advancements, critical limitations persist. First, we observed a divergence between quantitative metrics and perceptual quality; standard mIoU failed to capture significant improvements in boundary adherence and semantic consistency. Second, the semi-supervised approach occasionally underperformed supervised baselines, meaning adding unlabeled data to the equation didn’t benefit in some situations at all. Finally, while our model outperforms existing methods in cross-city generalization, zero-shot slum detection remains a non-trivial challenge that current state-of-the-art SSL methods struggle to solve in isolation. Future work must focus

on integrating multi-modal data to resolve the visual ambiguity between slums and formal housing that optical data alone cannot distinguish. Incorporating socioeconomic data coupled with geospatial indicators, such as wealth proxies and population density maps, is essential to enhance the differentiation capability of future models for informed urban planning.

### Declaration of Generative AI use

During the preparation of this work the authors used Google's Gemini and Openai's ChatGPT in order to refine the academic writing of the manuscript. After using this tool/service, the authors reviewed and edited the content as needed and takes full responsibility for the content of the published article.

### Declaration of competing interests

The authors declare that they have no known competing financial interests or personal relationships that could have appeared to influence the work reported in this paper.

### Funding

This work was supported by the German Academic Exchange Service under Project No. 57708351. The research was carried out at the German Research Center for Artificial Intelligence (DFKI GmbH, Kaiserslautern, Germany) and the National University of Sciences and Technology (NUST, Islamabad, Pakistan).

### Data Availability

All research assets required to replicate this study, including the new dataset in form of KML along with scripts to reproduce the dataset into image-mask pairs format, preprocessing workflows, model definitions, experimental pipelines and training logs, will be made publicly available after paper acceptance; currently, they can be provided upon a reasonable request. All other datasets cited are already publicly accessible [13, 14, 16].

### References

- [1] UN-Habitat, UN-Habitat Strategic Plan 2026-2029, Tech. rep., United Nations, Accessed: Dec. 20, 2025 (2025).  
URL [https://unhabitat.org/sites/default/files/2025/02/prefinal\\_draft\\_sp\\_2026-2029\\_v2\\_feb\\_18\\_approved.pdf](https://unhabitat.org/sites/default/files/2025/02/prefinal_draft_sp_2026-2029_v2_feb_18_approved.pdf)
- [2] UN-Habitat, From Housing Informality To Adequate Housing, Tech. rep., United Nations, Accessed: Dec. 20, 2025 (2025).  
URL [https://unhabitat.org/sites/default/files/2025/06/informal\\_settlements\\_-\\_background\\_paper\\_and\\_draft\\_recommendations.pdf](https://unhabitat.org/sites/default/files/2025/06/informal_settlements_-_background_paper_and_draft_recommendations.pdf)
- [3] United Nations Children's Fund (UNICEF), Coverage Survey in Slums of 10 Largest Cities of Pakistan, Tech. rep., UNICEF Pakistan, Accessed: Dec. 20, 2025 (2020). URL <https://www.unicef.org/pakistan/reports/coverage-survey-slumsunderserved-areas-10-largest-cities-pakistan>
- [4] Y. Zha, J. Gao, S. Ni, Use of normalized difference built-up index in automatically mapping urban areas from tm imagery, *International journal of remote sensing* 24 (3) (2003) 583–594.
- [5] M. Kawamura, S. Jayamanna, Y. Tsujiko, Quantitative evaluation of urbanization in developing countries using satellite data, *Doboku Gakkai Ronbunshu* 1997 (580) (1997) 45–54.
- [6] K. G. Alrasheedi, A. Dewan, A. El-Mowafy, Combining local knowledge with object-based machine learning techniques for extracting informal settlements from very high-resolution satellite data, *Earth Systems and Environment* 8 (2) (2024) 281–296. doi:10.1007/s41748-024-00393-1.
- [7] M. Sheykhmousa, M. Mahdianpari, H. Ghanbari, F. Mommadimanesh, P. Ghamisi, S. Homayouni, Support vector machine versus random forest for remote sensing image classification: A meta-analysis and systematic review, *IEEE Journal of Selected Topics in Applied Earth Observations and Remote Sensing* 13 (2020) 6308–6325. doi:10.1109/JSTARS.2020.3026724.
- [8] I. Lizarazo, Quantitative land cover change analysis using fuzzy segmentation, *International Journal of Applied Earth Observation and Geoinformation* 15 (2012) 16–27, special Issue on Geographic Object-based Image Analysis: GEOBIA. doi:10.1016/j.jag.2011.05.012.
- [9] T. Stark, M. Wurm, H. Debray, X. X. Zhu, H. Taubenböck, Uncertainty aware slum mapping in 55 heterogeneous cities, *International Journal of Applied Earth Observation and Geoinformation* 145 (2025) 104979. doi:10.1016/j.jag.2025.104979.
- [10] O. Ronneberger, P. Fischer, T. Brox, U-net: Convolutional networks for biomedical image segmentation, in: *International Conference on Medical image computing and computer-assisted intervention*, Springer, 2015, pp. 234–241. doi:10.1007/978-3-319-24574-4\_28.
- [11] M. Oquab, T. Darcet, T. Moutakanni, H. V. Vo, M. Szafraniec, V. Khalidov, P. Fernandez, D. HAZIZA, F. Massa, A. El-Nouby, M. Assran, N. Ballas, W. Galuba, R. Howes, P.-Y. Huang, S.-W. Li, I. Misra, M. Rabbat, V. Sharma, G. Synnaeve, H. Xu, H. Jegou, J. Mairal, P. Labatut, A. Joulin, P. Bojanowski, DINOv2: Learning robust visual features without supervision, *Transactions on Machine Learning Research* (2024). URL <https://openreview.net/forum?id=a68SUt6zFt>

[12] Google, Google Earth Pro V 7.3.6, Desktop application, Accessed Dec. 20, 2025 (2025).

[13] Slum Rehabilitation Authority, Mumbai, Mumbai - Slum Cluster Map, Accessed: Dec. 20, 2025 (2015). URL <https://data.opencity.in/dataset/mumbai-slum-cluster-map>

[14] Karachi Cartography, Katchi Abadi Map, Accessed: Dec. 20, 2025 (2024). URL <https://www.karachicartography.org/kachi-abadi-map/>

[15] Q. Wu, Leafmap: A python package for interactive mapping and geospatial analysis with minimal coding in a jupyter environment, *Journal of Open Source Software* 6 (63) (2021) 3414. doi:10.21105/joss.03414.

[16] B. J. Gram-Hansen, P. Helber, I. Varatharajan, F. Azam, A. Coca-Castro, V. Kopackova, P. Bilinski, Mapping informal settlements in developing countries using machine learning and low resolution multi-spectral data, in: *Proceedings of the 2019 AAAI/ACM Conference on AI, Ethics, and Society*, 2019, pp. 361–368. doi:10.1145/3306618.3314253.

[17] M. Batty, M. Longley, *Fractal cities - a geometry of form and function*, Academic Press, London (01 1994).

[18] M. M. Arif, O. Devisch, Y. Schoonjans, Examining the intricacies and perpetual issues in urban informal settlements: Lessons from two case studies of informal settlements in lahore, pakistan, *Journal of Art, Architecture and Built Environment* 6 (1) (2023) 62–93.

[19] A. Oliver, A. Odena, C. Raffel, E. D. Cubuk, I. J. Goodfellow, Realistic evaluation of deep semi-supervised learning algorithms, in: *Proceedings of the 32nd International Conference on Neural Information Processing Systems, NIPS'18*, Curran Associates Inc., Red Hook, NY, USA, 2018, p. 3239–3250.

[20] L. v. d. Maaten, G. Hinton, Visualizing data using t-sne, *Journal of machine learning research* 9 (Nov) (2008) 2579–2605.

[21] J. Lin, Divergence measures based on the shannon entropy, *IEEE Transactions on Information Theory* 37 (1) (1991) 145–151. doi:10.1109/18.61115.

[22] L. Yang, L. Qi, L. Feng, W. Zhang, Y. Shi, Revisiting weak-to-strong consistency in semi-supervised semantic segmentation, in: *2023 IEEE/CVF Conference on Computer Vision and Pattern Recognition (CVPR)*, 2023, pp. 7236–7246. doi:10.1109/CVPR52729.2023.00699.

[23] L.-C. Chen, Y. Zhu, G. Papandreou, F. Schroff, H. Adam, Encoder-decoder with atrous separable convolution for semantic image segmentation, in: *Proceedings of the European conference on computer vision (ECCV)*, 2018, pp. 801–818. doi:10.1007/978-3-030-01234-2\_49.

[24] K. Sohn, D. Berthelot, N. Carlini, Z. Zhang, H. Zhang, C. A. Raffel, E. D. Cubuk, A. Kurakin, C.-L. Li, Fixmatch: Simplifying semi-supervised learning with consistency and confidence, in: H. Larochelle, M. Ranzato, R. Hadsell, M. Balcan, H. Lin (Eds.), *Advances in Neural Information Processing Systems*, Vol. 33, Curran Associates, Inc., 2020, pp. 596–608.

[25] S. Yun, D. Han, S. Chun, S. J. Oh, Y. Yoo, J. Choe, Cutmix: Regularization strategy to train strong classifiers with localizable features, in: *2019 IEEE/CVF International Conference on Computer Vision (ICCV)*, 2019, pp. 6022–6031. doi:10.1109/ICCV.2019.00612.

[26] Y. Wang, H. Chen, Q. Heng, W. Hou, Y. Fan, Z. Wu, J. Wang, M. Savvides, T. Shinozaki, B. Raj, B. Schiele, X. Xie, Freematch: Self-adaptive thresholding for semi-supervised learning, in: *The Eleventh International Conference on Learning Representations*, 2023. URL [https://openreview.net/forum?id=PDrUPTXJI\\_A](https://openreview.net/forum?id=PDrUPTXJI_A)

[27] L. Yang, Z. Zhao, H. Zhao, Unimatch v2: Pushing the limit of semi-supervised semantic segmentation, *IEEE Transactions on Pattern Analysis and Machine Intelligence* 47 (4) (2025) 3031–3048. doi:10.1109/TPAMI.2025.3528453.

[28] K. He, X. Zhang, S. Ren, J. Sun, Deep residual learning for image recognition, in: *2016 IEEE Conference on Computer Vision and Pattern Recognition (CVPR)*, 2016, pp. 770–778. doi:10.1109/CVPR.2016.90.

[29] R. Ranftl, A. Bochkovskiy, V. Koltun, Vision transformers for dense prediction, in: *2021 IEEE/CVF International Conference on Computer Vision (ICCV)*, 2021, pp. 12159–12168. doi:10.1109/ICCV48922.2021.01196.

[30] A. Dosovitskiy, L. Beyer, A. Kolesnikov, D. Weissenborn, X. Zhai, T. Unterthiner, M. Dehghani, M. Minderer, G. Heigold, S. Gelly, J. Uszkoreit, N. Houlsby, An image is worth 16x16 words: Transformers for image recognition at scale, in: *International Conference on Learning Representations*, 2021. URL <https://openreview.net/forum?id=YicbFdNTTy>